Local density of states analysis using Bader decomposition for N_2 and CO_2 adsorbed on Pt(110)-(1 × 2) electrodes

Sigrídur Gudmundsdóttir,[1] Wenjie Tang,[2] Graeme Henkelman,[2] Hannes Jónsson,[1] and Egill Skúlason[1]
[1]*Science Institute and Faculty of Science, VR-III, University of Iceland, 107 Reykjavík, Iceland*
[2]*Chemistry Department, University of Texas, Austin, Texas 78712, USA*

(Received 6 July 2012; accepted 8 October 2012; published online 29 October 2012)

Local density of states and electric charge in regions defined for individual atoms and molecules using grid based Bader analysis is presented for N_2 and CO_2 adsorbed on a platinum electrode in the presence of an applied electric field. When the density of states is projected onto Bader regions, the partial density of states for the various subregions correctly sums up to the total density of states for the whole system, unlike the commonly used projection onto spheres which results in missing contributions from some regions while others are over counted, depending on the radius chosen. The electrode is represented by a slab with a missing row reconstructed Pt(110)-(1 × 2) surface to model an edge between micro-facets on the surface of a nano-particle catalyst. For both N_2 and CO_2, a certain electric field window leads to adsorption. The binding of N_2 to the electrode is mainly due to polarization of the molecule but for CO_2 hybridization occurs between the molecular states and the states of the Pt electrode. © *2012 American Institute of Physics*. [http://dx.doi.org/10.1063/1.4761893]

I. INTRODUCTION

Atomic scale simulations of electrochemical processes is an important and growing research area. While electrochemistry has played a vital role in the development and formulation of chemical concepts, modern atomic scale studies of electrochemical processes have been rather limited. On the experimental side, the challenge is to characterize processes at a solid/liquid interface as a function of applied voltage, a complex system where few experimental techniques can be applied. On the theoretical side, simulations of such systems require an accurate description of the electronic properties of systems including a large number of atoms. As a result, the calculations require large computational effort. Furthermore, it is not clear how to best describe electrochemical systems in atomistic simulations. Several approaches have been proposed.[1–9] In most of these, the electrode is represented by a slab of material subject to periodic boundary conditions in two dimensions, typically a metal, and the solution is represented by a thin layer of water molecules, typically arranged in an ice structure. In some cases, counter ions have been included.

An important question is how applied voltage affects the binding of molecules to the electrode surface. Calculations addressing this question have previously been carried out by applying a constant electric field using a sawtooth external potential.[10–15] The metal slab responds to the applied electric field by transferring electrons from one side of the slab to the other. This can be seen in Fig. 1. The methodology for doing this is already in place in many software applications used for surface science calculations because of the need to cancel out surface dipoles. We apply this technique here to study the adsorption of N_2 and CO_2 on a Pt electrode. The electronic interaction of N_2[15–19] and CO_2[17,20–24] molecules with surfaces has been studied extensively with electronic structure calculations in the context of, e.g., chemical sensors and catalysis. In order to analyze the effects of an electric field, a decomposition of the continuous electron density in the system is needed to extract useful indicators of charge transfer and modifications of chemical properties. We have made use of the charge density decomposition defined by Bader[25] and describe below our implementation of local density of state (DOS) analysis within regions assigned in this way to atoms and/or molecules. There, surfaces are placed where the electron density is minimal to divide space into regions which can in most cases be associated with atoms. More precisely, the dividing surfaces are placed in such a way that the gradient of electron density has zero component normal to the surface, i.e., these are zero-flux surfaces.

Several different approaches have been used in the implementation of Bader analysis. Early algorithms were designed for quantum chemistry calculations of small molecules where the gradient of the charge density can be calculated from derivatives of an analytical wave function.[25–27] Stationary points of the charge density are first identified and paths along the density gradient then followed from these points to map out the connectivity of the stationary points and locate the zero-flux dividing surfaces. The total number of electrons in each Bader region is then obtained by radial integration from the charge density maximum to the surface. While this approach works for small molecules, a high density of paths is needed to accurately represent the surface away from the critical points. The method requires large computational effort for large systems.[28] It has also been found to be unreliable for complex bonding geometries. The radial integration rays can, in particular, have multiple intersection points with the dividing surface. Several improvements to this original approach have been proposed. Popelier developed a method to more accurately integrate the charge density within each Bader region

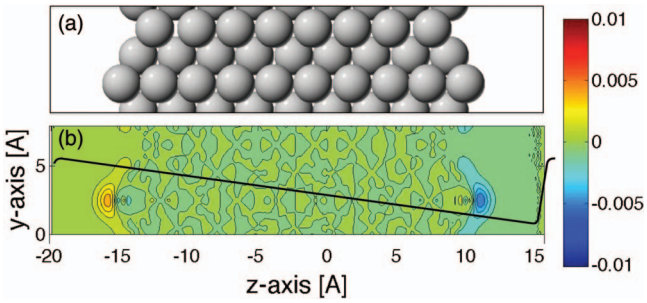

FIG. 1. (a) Side view of the Pt(110)-(1×2) slab with 18 layers used in the DFT calculations. (b) The change in electron density when a constant electric field of −0.5 V/Å is applied over the slab. The color scale is in e/A^3. The integrated charge transfer from one side of the slab to the other is 0.25 electrons with −0.5 V/Å field applied. The sawtooth potential which is applied to the system is shown with a black line. The local electric field inside the metallic slab is zero (not shown). The change in electron density is calculated by subtracting the total electron density for each grid point without applied electric field from the total electron density with applied electric field. The electron density difference is averaged along the direction of the ridges on the Pt(110)-(1×2) surface.

using a Fourier-Chebyshev fit[29] and a bisection method to analytically represent the dividing surfaces.[30] Other approaches suggested by Popelier include the use of the divergence theorem to replace the three-dimensional integration over the Bader regions into a two-dimensional integral over the dividing surfaces,[28] and the use of a tree search to treat complex bonding topologies between critical points.[31] Another quite different approach is to form an elastic sheet along the zero-flux surfaces.[32]

Many current applications of Bader's analysis involve a grid of numerical charge density values on a grid as input.[26,33–35] This is in particular the case for plane-wave-based density functional theory (DFT) calculations, the most common methodology used in computational studies of condensed phase systems. Instead of analytical functions, the algorithm for finding the zero-flux surfaces can be strictly based on the input grid points.[34] In the original formulation of this algorithm, paths through the grid points following maximal increase in charge density were constructed to assign the grid points to Bader regions. By making use of bookkeeping, each grid point needs to be considered only once. The method is efficient, scales linearly with system size, and can deal with complex bond topology. The original algorithm has, however, been shown by Sanville *et al.*[35] to include a bias towards aligning the zero-flux surfaces with the lattice. A modified algorithm was implemented by the authors in which ascent trajectories along interpolated gradients of the charge density were not constrained to the grid. This algorithm removes the bias and retains the linear scaling of the original method. A modification of the original grid based algorithm has also been presented.[36] There, the lattice bias is removed by introducing a correction vector pointing from the nearest grid point to the unbiased, off-lattice path. This revised algorithm retains the efficiency, linear scaling, and robustness of the original, grid based method. Recently, Yu and Trinkle presented another improvement of the grid based algorithm which makes the integration over Bader regions more accurate for a given grid spacing.[37]

In this article, an extension of the grid based implementation is presented which makes it possible to decompose the DOS into a partial DOS for each Bader region. This represents further development of the previously described grid based Bader analysis software.[34,36,38] To illustrate the applicability, we discuss calculations of two systems, an adsorbed N_2 molecule and an adsorbed CO_2 molecule on the missing row reconstructed Pt(110)-(1 × 2) surface. The electrochemical reduction of these molecules to NH_3 and CH_3OH is of great interest. The former as a way of making fertilizer at ambient conditions, an alternative to the large scale industrial process of Haber-Bosch (for a recent theoretical study, see Ref. 15), and the latter for harvesting CO_2 from the atmosphere to make fuel (for a recent theoretical study, see Ref. 24). We choose this surface because it can be taken to be a model of a junction between micro-facets on a nanoparticle catalyst. The ridge sites formed at the Pt(110)-(1 × 2) surface are particularly reactive and represent an edge between (111) micro-facets.[39,40]

II. METHODOLOGY

A. Projection of DOS onto Bader regions

To calculate the local density of states (LDOS), the charge density of each electronic eigenstate $\rho_i(r)$ is projected onto the Bader regions

$$w_{J,i} = \int_r \Omega_J(r)\,\rho_i(r)\,dr, \tag{1}$$

where $\Omega_J(r)$ has the value 1 inside the Bader region with index J and 0 outside. The local DOS within the Bader region is then the total DOS multiplied by the projection weight $w_{J,i}$ for each state,

$$\mathrm{DOS}_J(\epsilon) = \sum_i \delta(\epsilon_i - \epsilon)\,w_{J,i}, \tag{2}$$

where ϵ_i is the energy of eigenstate i. In practice, some broadening is applied to the delta function to compare with experiment. Since the Bader regions fill space, the sum of the projection weights for each of the states is unity,

$$\sum_J w_{J,i} = 1, \tag{3}$$

so that the sum of the local DOS in the Bader volumes is equal to the total DOS.

The local DOS is calculated using an extension to our Bader analysis software.[38] In addition to the total charge density, the charge density for each eigenstate needs to be written in a uniform grid by the electronic structure code. Each grid point is assigned to a Bader volume by following a gradient ascent path along the total charge density. These volumes are stored so that any other charge density can be analyzed according to the Bader partitioning. Specifically, the charge density associated with each eigenstate is integrated over each Bader volume. In this way, each state is analyzed to give the weights from Eq. (1). Combining the contribution from each eigenstate in a Bader volume gives the local DOS as defined in Eq. (2). It is also possible to automate this procedure and avoid writing charge density files for electronic

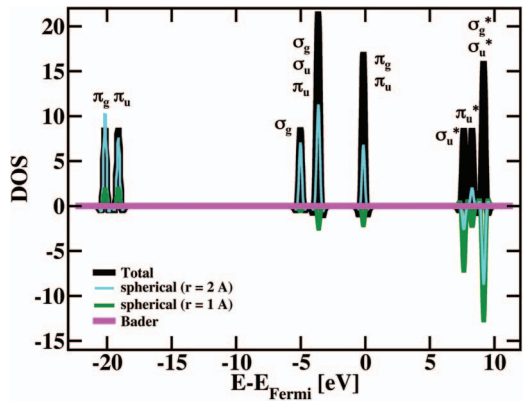

FIG. 2. Total density of electronic states, DOS, (black) for an isolated linear CO_2 molecule calculated using the DFT/RPBE approximation. Difference between the sum of partial DOS projected onto Bader regions for the atoms and the total DOS (magenta), and the difference between the sum of DOS projected onto spherical regions around the atomic nuclei using a radius of 1.0 Å (green), or 2.0 Å (cyan) and the total DOS. When Bader regions are used, the sum over the partial DOS is the same as the total DOS, but the use of spherical regions for the projection results in under counting and/or over counting and a significant error when the partial DOS are summed up and compared to the total DOS. The magnitude of, e.g., the lowest energy peaks (π_g and π_u) are about two times greater when using a sphere of 2.0 Å radius than the total DOS.

structure codes which can calculate or read the Bader partitioning information $\Omega_J(r)$ such as VASP.[41–44]

A simple illustration of the advantage of projecting onto the Bader regions instead of the more common approach of projecting onto spheres is shown in Fig. 2. The calculation is for a single CO_2 molecule. The sum over the partial DOS for the C-atom and the two O-atoms agrees well with the DOS for the whole molecule when the Bader regions are used. But, when the DOS is projected onto atom-centered spheres with a radius of 1 Å, the sum of DOS for the highest energy states (between +7.5 and +9 eV) is significantly smaller than the total DOS for the molecule, while the sum is slightly larger (at around −20 eV) or slightly smaller (−3.5 and 0 eV) for the lower energy states. Increasing the radius to 2 Å, increases the over counting significantly for the occupied states while the under counting for the unoccupied states is reduced slightly. For many of the occupied states, the sum over the partial DOS for the 2 Å case is twice the magnitude compared to the total DOS, illustrating the problem of the state-of-the-art method of projecting onto spherical regions. It is clear that no value of the radius will bring the sum over partial DOS into agreement with the DOS for the molecule as a whole.

B. The DFT calculations

The calculations presented here were carried out using density functional theory[45] as implemented in DACAPO[46] and VASP.[41–43] The calculations of the DOS projection onto both Bader regions and spherical regions were done with VASP, whereas calculations of the binding energy and other analysis of the charge localization were done using DACAPO. The RPBE functional approximation[47] was used. A plane wave basis set was used with a PAW representation of the core electrons[48] in the VASP calculations whereas ultra-soft pseudo-potentials were used in the DACAPO calculations. The plane wave cutoff was 33 Ry for the wave function and 41 Ry or 47 Ry for the density, depending on whether N_2 or CO_2 was in the system, respectively. We note that this level of theory does not properly take into account the long range dispersion forces. The total electron density used in the Bader analysis includes the contribution from the core electrons. The self-consistent electron density is determined by iterative diagonalization of the Kohn-Sham Hamiltonian, with the occupation of the Kohn-Sham states being smeared according to a Fermi-Dirac distribution with a smearing parameter of $k_BT = 0.1$ eV. All calculated values of the energy have been extrapolated to $k_BT = 0$ eV.

The electrode was represented by a Pt slab with missing-row reconstructed (110)-(1 × 2) surface. The calculated optimal lattice constant for the FCC structure, 4.02 Å, was used. The repeated supercell was three atoms wide in the direction along the ridge (x-direction) and four atoms wide in the y-direction, see inset in Fig. 3(b). A total of 8 Pt layers were included in the calculations where either N_2 or CO_2 was adsorbed on the top most Pt atoms of the ridge on the surface. The four bottom metal layers were fixed and the four top layers were allowed to relax as were the adsorbed species. Configurations were optimized with respect to coordinates of movable atoms until atomic forces were less than 0.01 eV/Å. Monkhorst-Pack k-point sampling of 4 × 4 × 1 was used and maximum symmetry was applied to reduce the number of k-points in the calculations. The slabs were separated by approximately 12 Å of vacuum.

III. RESULTS AND DISCUSSIONS

A. N_2 adsorption

The N_2 molecule binds most strongly on top of a ridge atom on the Pt(110)-(2×1) surface with the molecular axis directed along the surface normal. Binding at a bridge site on the ridge results in a slightly lower binding energy. A stable binding site for the N_2 molecule lying flat along the ridge was not found in these DFT/RPBE calculations, but the long range dispersion interaction is not included at this level of approximation.

The binding energy was calculated as a function of applied electric field using

$$\Delta E_{N_2} = E_{Pt-N_2,field} - E_{Pt,field} - E_{N_2}, \quad (4)$$

where the same field is applied to the surface with and without adsorbed N_2, but the isolated N_2 molecule is in vacuum without a field. The results are shown in Fig. 3(a). At zero field, the binding energy is 0.31 eV and an integration of the electron density in the Bader region shows that a charge transfer of 0.17 electrons occurs from the surface to the molecule.

When an electric field is applied, a parabolic dependence of the binding energy is obtained, characteristic of polarization. A dipole moment $\mu = \alpha\epsilon$ is induced in a molecule with polarizability α in a field ϵ and the energy is then lowered by

$$E = -\frac{1}{2}\alpha\epsilon^2. \quad (5)$$

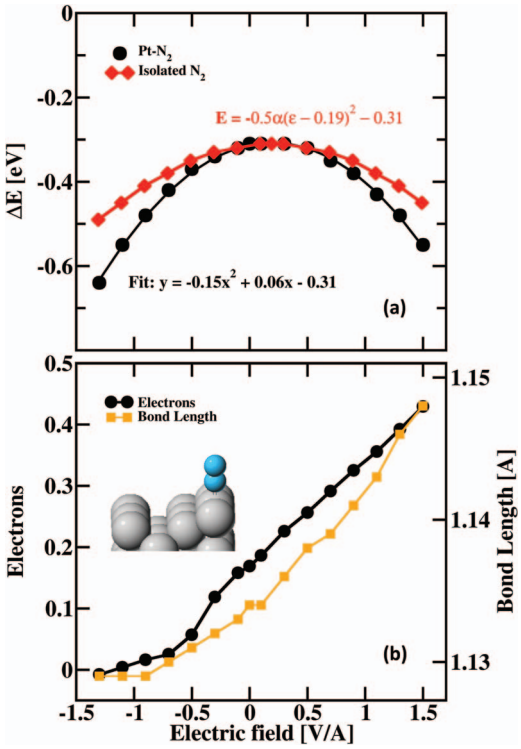

FIG. 3. (a) Binding energy (black circles) of an N_2 molecule on the ridge of the Pt(110)-(1×2) surface (see inset in (b)) as a function of applied electric field. The binding energy is calculated with respect to N_2 in the gas phase without applied field and a clean slab with the field applied, see Eq. (4). The polarization energy (red diamonds) of the N_2 molecule in vacuum is shown for comparison. It is calculated by subtracting the energy of N_2 in an applied field from the N_2 in the absence of the field. (b) The change in integrated electron density in the Bader region of the N_2 molecule and the N-N bond length as a function of the applied electric field. In the absence of an external field, about 0.17 electrons are transferred to the lower N-atom of the N_2 molecule from the underlying Pt-atom (see also Fig. 4) and this creates an electrical field that polarizes the molecule. A small positive applied field cancels out this local field and the maximum of the polarization parabola in (a) is, thereby, shifted to +0.19 V/Å. Between the interval of −0.5 V/Å and +0.9 V/Å of the applied field, the binding of the N_2 molecule to the surface can be described as a constant contribution of about 0.3 eV independent of the field, plus a small contribution due to polarization. For larger values of the field, the binding energy of the N_2 molecule increased significantly because of the polarization of the N_2 molecule. The adsorbed N_2 molecule has nearly twice as large polarizability than the isolated molecule. Inset: Tilted side view of a N_2 molecule adsorbed on the ridge on the Pt(110)-(1×2) surface.

For an isolated N_2 molecule, the energy difference $E_{N_2} - E_{N_2,field}$ was calculated as a function of the applied field. The curvature gives the polarizability of the isolated N_2 as 2.59×10^{-40} $C^2m^2J^{-1}$. The gas phase N_2 molecule has an experimentally determined polarizability of 1.97×10^{-40} $C^2m^2J^{-1}$. Hence, the DFT value is about 30% greater than the experimental value, a typical overestimation in DFT-GGA of the polarizability. The calculated polarization energy of an N_2 molecule in vacuum is shown in Fig. 3(a) and can be compared directly with the calculated binding energy of the N_2 molecule at the Pt(110)-(1×2) surface. A parabolic dependence of the energy with the field is observed both for the isolated molecule and for an admolecule on the electrode, showing that the main effect of the applied field on the binding energy is due to polarization of the molecule. The polarization is, however, nearly two times greater when N_2 is adsorbed on the Pt(110)-(1×2) surface as compared to an isolated molecule. Interestingly, an N_2 molecule at the Pt(111) surface is calculated to have the same polarizability as an isolated N_2 and the molecule does not bind to the (111) surface at moderate field values. Apparently, the binding of the N_2 molecule at the ridge on the Pt(110)-(1×2) surface increases the polarizability of the molecule and this results both in stronger adsorption energy when no field is applied and makes the effect of the applied field stronger.

The polarization parabola in Fig. 3(a) is shifted so that the maximum is at a field of +0.19 V/Å. This is likely due to a local field that is formed by the electron transfer from the ridge Pt-atom to the lower N-atom which is evident in Fig. 4. An external field of +0.19 V/Å cancels this local field and thereby leads to minimal binding of the molecule to the surface.

For positive field, the electron transfer is nearly linearly related to the magnitude of the applied field, as shown in Fig. 3(b). This correlates nicely with an elongation of the N-N bond, as expected. For negative field, the behavior is more complex and a particularly rapid decrease in the electron transfer occurs at around −0.4 V/Å. At an applied field of −1 V/Å, the field has opposed the tendency for electron transfer to the N_2 molecule and no net electron transfer to the Bader region associated with the N_2 molecule occurs and as the magnitude of the field is increase further, the N-N bond length stays constant. The Pt-N distance (not shown) decreases almost linearly when the electric field is increased, from 2.07 Å at −1.5 V/Å to 1.98 Å at 0 V/Å to 1.93 Å at +1.5 V/Å, or by 0.14 Å in total.

The change in the charge density, $\Delta\rho$, upon adsorption was calculated using

$$\Delta\rho = \rho_{Pt-N_2,field} - \rho_{Pt,field} - \rho_{N_2,field} \quad (6)$$

and the results are shown in Fig. 4. In addition to the zero field case, the charge density change upon adsorption in the presence of large positive and large negative field was also calculated. The same field is then applied to the isolated N_2 molecule as the slab with and without an admolecule. The adsorption of the N_2 molecule results in a decrease in the electron density of the underlying Pt-atom. The shape of the contours indicates that the electrons are coming from the d_z^2 orbital. With a positive field applied, the depletion of electron density at the Pt atom becomes larger, while it decreases for a negative field. This is in agreement with the number of electrons in the Bader region of N_2, shown in Fig. 3(b). The contours around the N_2 molecule show the polarization of the molecule. In all cases, the system is polarized as discussed previously, even when no field is applied. For all values of the field, charge depletion is induced at the end of the nitrogen atom which is in contact with the Pt atom underneath. Since charge is also depleted from the underlying Pt-atom, the bond between the N_2 molecule and the Pt electrode is not a purely ionic bond. This confirms our previous conclusions that the variation in the adsorption energy in Fig. 3(a) is mainly because of the polarization of the N_2 molecule.

The LDOS, i.e., DOS projected onto the Bader region of the N-atom (of the adsorbed N_2 molecule) which is in contact with the Pt surface, is shown in Fig. 5(b). For comparison, the

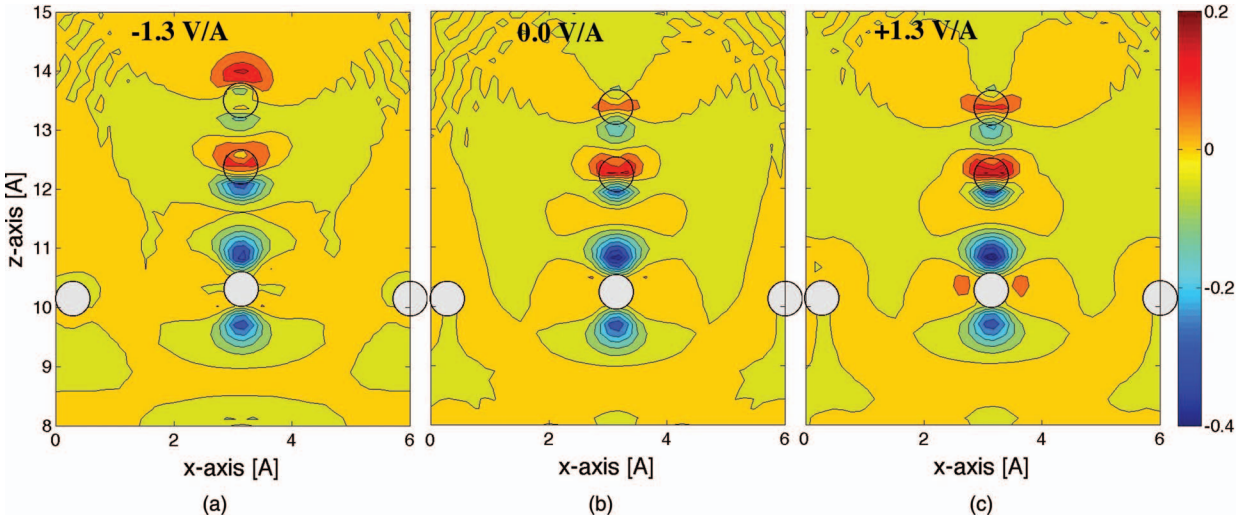

FIG. 4. The electron density difference between an N_2 molecule adsorbed on the Pt(110)-(1×2) surface and an isolated N_2 molecule plus a clean surface, see Eq. (6). The molecule sits on-top of a ridge Pt-atom as shown in the inset of Fig. 3. The electron density difference, $\Delta\rho$, is averaged over a thin slice (a few grid points) in the y-direction. The middle of this slice includes the line running through the Pt ridge atoms and the axis of the N_2 molecule. (a) With an applied electric field of −1.3 V/Å, (b) no field, and (c) with an applied electric field of +1.3 V/Å. The grey filled circles show the position of the Pt ridge atoms whereas the open circles indicate the position of the N_2 molecule. When an electric field is applied, the same field is applied to the slab with and without N_2 and the isolated N_2 molecule.

DOS of one of the N-atom when a N_2 molecule is far away from the Pt slab, placed in the vacuum region, is also shown in Fig. 5(a). The Pt slab is included in both calculations to fix the Fermi level, thereby obtaining a common reference energy. The Fermi level is then close to midway between the HOMO and LUMO of the molecule. When a calculation is carried out for just a single N_2 molecule, the "Fermi level" is, however, set right above the energy of the HOMO. A comparison between a calculation with and without a slab would then indicate a large shift in all the orbital energies with respect to the Fermi level, simply because the Fermi level is different. Such large shifts have, in fact, been noted in the literature.[49,50]

Fig. 5(b) shows the effect of the applied field on the LDOS of the adsorbed N_2 molecule. While the energy of the two lowest states (σ_g and σ_u^*) is a monotonic function of the applied field, the higher energy states show no clear trend when the field is varied. Some of the shifts can be related to the charge transfer, see inset in Fig. 5(a). This can be seen by adding some charge, consistent with the Bader charge analysis shown in Fig. 3(b), to the gas phase N_2 molecule. For values of the electric field; −0.5, 0, and +0.5 V/Å, the Bader analysis shows 0.06, 0.17, and 0.26 electrons transferred to the N_2 molecule from the Pt slab, respectively. The additional electrons are localized at the molecule. To keep charge neutrality of the simulated cell, a uniform positive charge background is included when electrons are added to the system. This charge is distributed uniformly over the whole simulation cell. The DOS for a charged, isolated molecule shows the same monotonic energy shift for all the peaks (except for the unoccupied peak at +5 eV) as obtained for the states at −24 eV and −12 eV when the molecule is adsorbed on the Pt electrode. This shows that these energy shifts are caused by the charge transferred to the molecule and not because of the electric field directly or hybridization with Pt states. The HOMO-2 σ_u^* state is, however, clearly also shifted down in energy with respect to the Fermi level when the nitrogen molecule is adsorbed on the Pt surface which indicates that there is also some hybridization with the Pt d-states. This state from the nitrogen molecule is clearly seen in the Bader region of the underlying Pt-atom, between −12.5 and −10 eV in Fig. 5(c). Such a hybridization has been discussed previously for N_2 on IrO_2 in the absence of an electric field.[18] The charge transfer to the nitrogen molecule can, however, not explain the more complicated shifts in the HOMO-1, HOMO, and the LUMO peaks where hybridization with the Pt states may play a greater role. The electrons in the HOMO σ_g state can overlap with the Pt d-states (Figs. 5(b) and 5(c)).

B. CO_2 adsorption

For the adsorption of a CO_2 molecule on the ridge of the Pt(110)-(2×1) surface, there are several possible bonding configurations as shown in Fig. 6. Five stable arrangements have been found with lower energy than clean surface and a CO_2 molecule in gas phase for some range of the applied field. For a positive electric field of 0.5 V/Å or higher, three bent configurations of the molecule involving bonding of the C-atom to a Pt-atom have been found. In one of these, an O-atom is also bonded to a neighboring Pt-atom. This turns out to be the strongest bonding configuration, as shown in Fig. 7(a), but it is only slightly more favorable than the other two. Appreciable charge transfer occurs from the surface to the molecule in these cases, amounting to 0.35 electrons to 0.7 electrons, depending on the strength of the field, as shown in Fig. 7(b). The bending of the CO_2 molecule induces a dipole moment which contributes to the bonding to the surface. Such bending has been noted in previous simulation studies,[17,20–22] in particular for CO_2 adsorption on the Cu(211) surface in a charged electrochemical double layer.[51] The binding energy was calculated in a similar way as in Eq. (4).

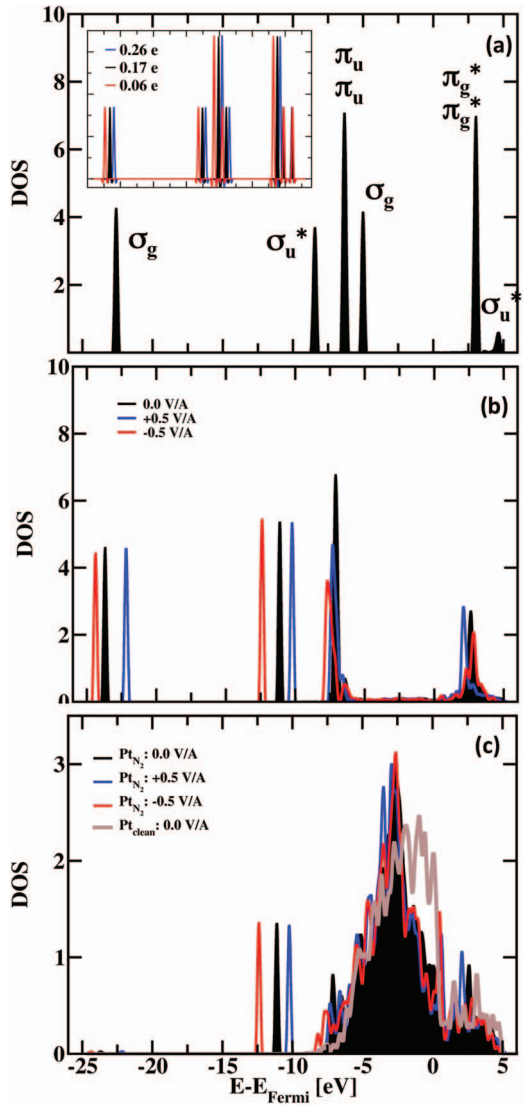

FIG. 5. (a) The density of states of an N atom in a N_2 molecule placed high above the Pt(110)-(1×2) surface. Inset: DOS of isolated N_2 with varying number of electrons corresponding to the calculated electron transfer to the N_2 admolecule in Fig. 3(b). (b) DOS projected onto the Bader region corresponding to the N-atom which is bound to a Pt-atom when the N_2 molecule is adsorbed on the Pt(110)-(1×2) surface in applied field of −0.5 V/Å (red), no field (black), and +0.5 V/Å (blue). (c) Similar as in (b) whereas here the DOS is projected onto the Bader region corresponding to the Pt atom in contact with the N_2 molecule, or when the Pt surface is clean (brown). The energy on the horizontal axis is given with respect to the Fermi level.

For negative field and up to zero field, two bonding configurations have been found where a linear CO_2 molecule points along the surface normal. In one case, the lower O-atom is sitting atop a Pt-atom on the ridge. In the other, it sits on a bridge site, see Fig. 6 (configurations (d) and (e)). These correspond to a polarization interaction, analogous to what was observed for the N_2 molecule, but without appreciable charge transfer between the surface and the molecule. The binding energy can become quite large for a large field because of the large polarizability of the CO_2 molecule along the molecular axis.

The change in the charge density upon adsorption, calculated using Eq. (6), is shown in Fig. 8. The largest increase is at the C-atom in the region of the bond with the Pt-atom

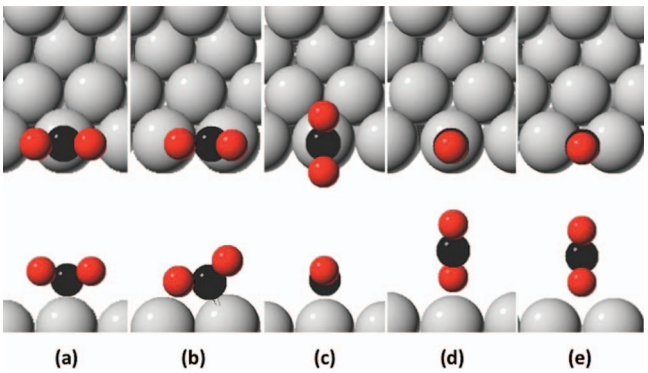

FIG. 6. Top view (upper) and side view (lower) of a CO_2 molecule adsorbed in various positions on the Pt(110)-(1×2) surface. All five configurations shown are lower in energy than a clean surface plus gas phase CO_2 for some range in the applied electric field, see Fig. 7.

(configurations (a) and (b)). Charge accumulates around the C-atom and significant decrease in electron density is found at the underlying Pt-atom, implying an interaction with ionic character. Even in the case where one of the O-atoms comes close to a neighboring Pt-atom (configuration (b)), there is not an appreciable net increase in electron density at the O-atoms. A stronger positive electric field leads to larger transfer of electrons and the charge accumulation at the C-atom and depletion at the Pt-atom becomes more pronounced. This is in agreement with the electron transfer to the CO_2 molecule obtained with the Bader analysis shown in Fig. 7(b).

In Fig. 9 the LDOS for the CO_2 molecule is shown. The linear CO_2 molecule is placed in the vacuum region and the

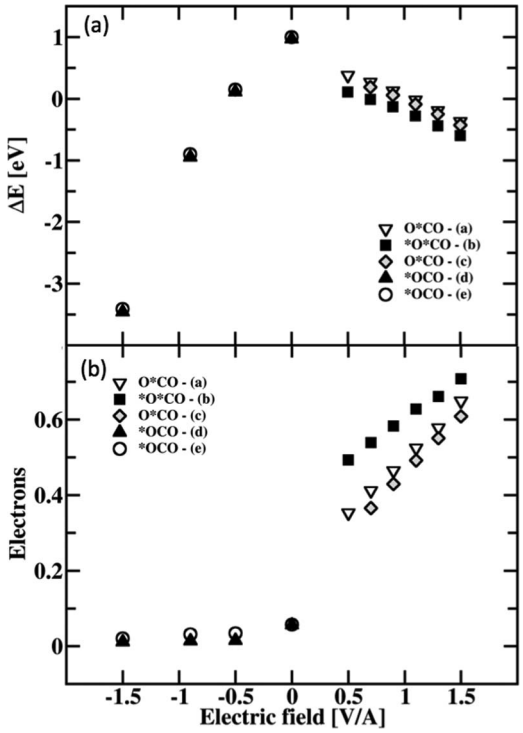

FIG. 7. (a) Adsorption energy of a CO_2 molecule in various configurations on the Pt(110)-(1×2) surface as a function of the applied electric field. The adsorption energy was calculated with Eq. (4), where the gas phase molecule is not in an electric field whereas the slab with and without admolecule is in the field. (b) The integrated transfer of electrons to the Bader region of the adsorbed CO_2 molecule as a function of the applied electric field.

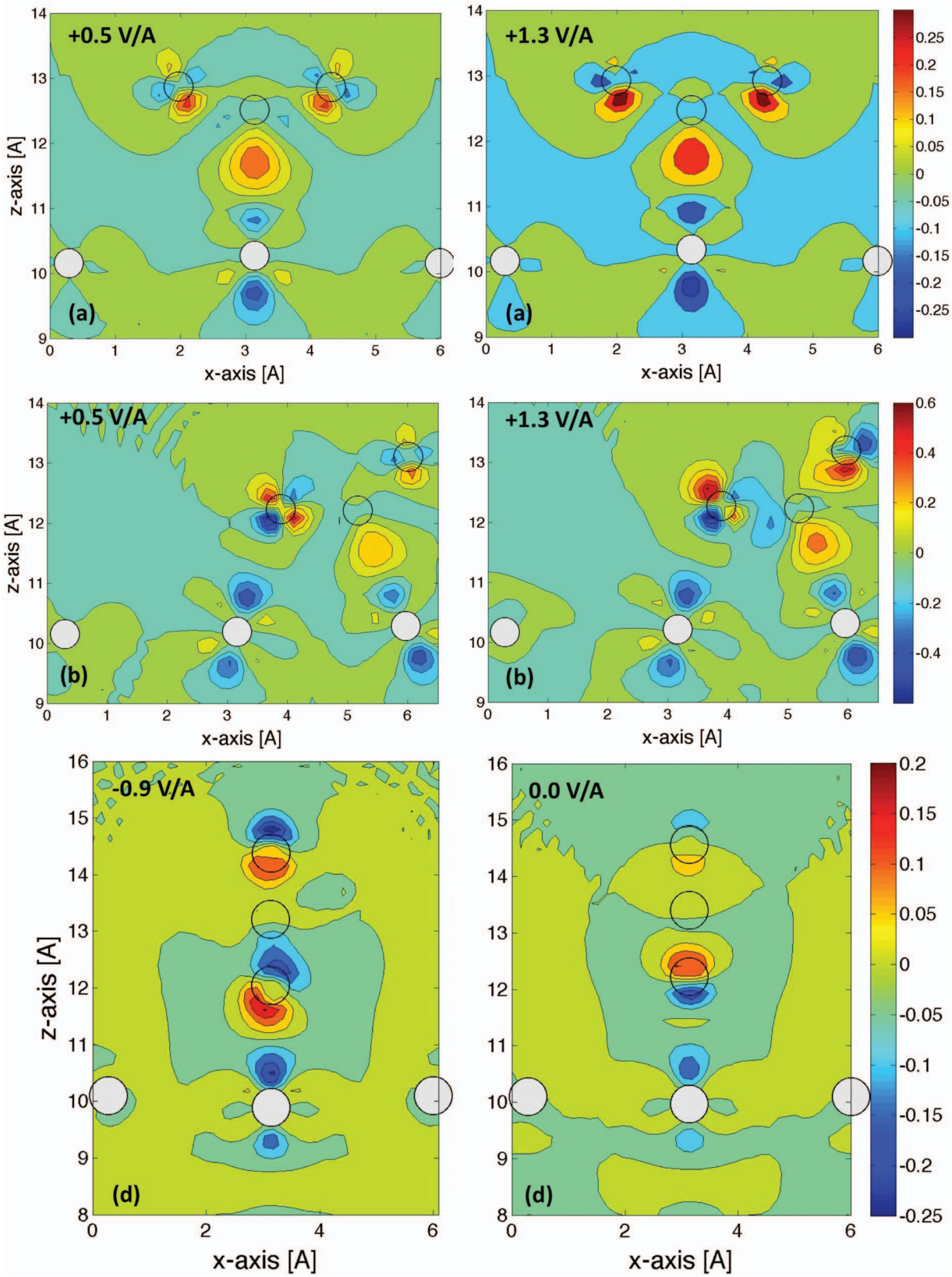

FIG. 8. Electron density difference (similar to Eq. (6)) for an adsorbed CO_2 on the Pt(110)-(1×2) surface in configurations shown in (a), (b), and (d) of Fig. 6 averaged over a thin slice (a few grid points) of the y-direction. The middle of this slice includes the line going through the Pt ridge atoms and the CO_2 molecular axis. The applied electric field is +1.3 V/Å and +0.5 V/Å for configurations (a) and (b), but −0.9 V/Å and 0 V/Å for configuration (d). The same electric field is applied to the slab with and without CO_2 and to the isolated CO_2 molecule.

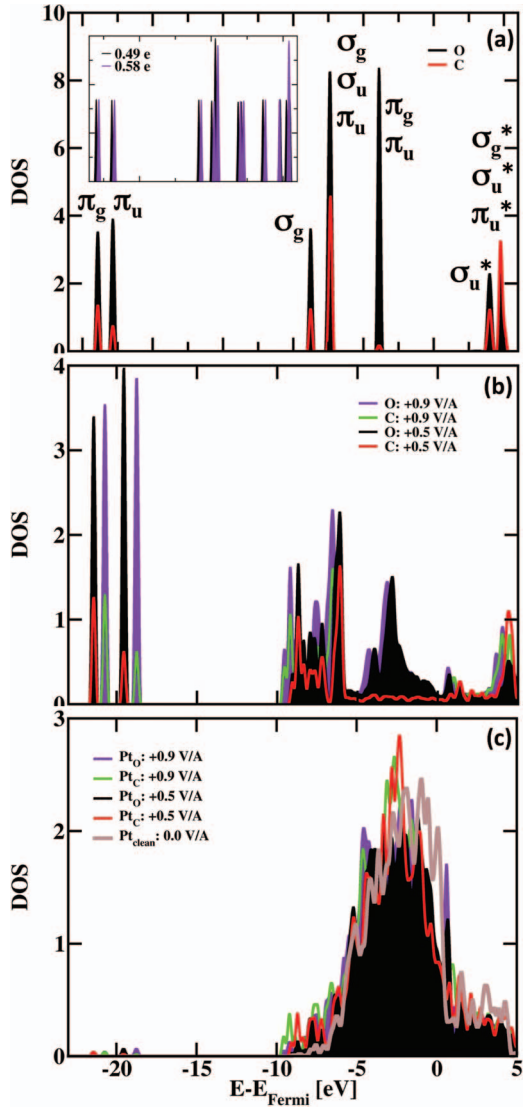

FIG. 9. (a) The density of states projected onto the Bader region of the C-atom and one of the O-atom of a CO_2 molecule placed high above the Pt(110)-(1×2) surface. Inset: DOS for isolated, bent CO_2 with varying number of electrons added. (b) DOS projected onto the Bader region of the C-atom and the lower O-atom which is in contact with a Pt-atom for a CO_2 molecule adsorbed in configuration (b) when the applied field is +0.5 V/Å (black for O-atoms and red for C-atoms) and +0.9 V/Å (violet for O-atoms and green for C-atoms). (c) Similar as in (b) for the DOS projected onto the Bader region corresponding to the Pt atom in contact with the C-atom and the O-atom, or when the Pt surface is clean (brown). The energy on the horizontal axis is given with respect to the Fermi level.

Pt slab is included in the calculation to ensure that the Fermi level is the same as when the molecule is adsorbed on the surface. This can be compared with the DOS for an isolated molecule in Fig. 2 where the Fermi level is set right above the HOMO. In the inset of Fig. 9(a), the effect of bending the gas phase CO_2 molecule to the shape of the adsorbed molecule can be seen. The degenerate peaks of σ_g, σ_u at −7.5 eV and π_g, π_u at −4 eV and σ_g^*, σ_u^* at +4 eV split when the CO_2 molecule is bent in agreement with Wang *et al.*[20]

Unlike the N_2 case, there is more pronounced chemical bonding between the bent CO_2 and the surface, as can be seen from the LDOS in Fig. 9(b). For the higher energy range, above −10 eV, there is clear signature of the presence of Pt states in the Bader region of the CO_2 molecule. Similarly, the molecular states can been seen in the LDOS of the Pt atoms in contact (Fig. 9(c)). This shows that the molecular states and surface Pt-states are mixed. By comparing with the gas phase DOS in Fig. 9(a), it is clear that the three higher energy states below the Fermi level are multiply split by hybridization with the Pt-states.

Electron transfer to an isolated CO_2 molecule shifts all the electronic states up in energy, as shown in the inset of Fig. 9(a). The same shift is observed for the CO_2 molecule when it is adsorbed on the Pt surface and an electric field is applied. This is, however, only visible in Fig. 9(b) for the states at around −20 eV, since they are not taking part in the hybridization with the surface. All the other molecular states hybridize with the Pt-states which leads to a downward shift in energy. Stronger positive field results in more hybridization as can be seen by comparing results from +0.9 V/Å with those from +0.5 V/Å. The binding energy of the CO_2 molecule also becomes larger as the electric field gets stronger, as shown in Fig. 7(a).

IV. SUMMARY

The calculations presented here demonstrate the use of Bader analysis in the study of electrochemical adsorption. In particular, the charge transfer can be deduced as a function of the applied electric field. Also, a new procedure is introduced for finding the local density of states corresponding to an atom by projecting onto the corresponding Bader region. This can be a useful tool for analyzing chemical bonding and it is applied here to a study of the interaction of admolecules with a surface. The effect of an applied field on the interaction of an N_2 molecule with the ridge on the (110)-(2×1) surface a Pt electrode was found to be mainly due to polarization of the molecule, but some hybridization between N_2 and Pt states is observed from the LDOS. For a CO_2 molecule, however, the hybridization with the Pt states is much stronger and can result in various chemical bonding arrangements of the admolecule.

ACKNOWLEDGMENTS

We would like to thank Jens K. Nørskov for many helpful discussions. G.H. would like to acknowledge support from the National Science Foundation under Grant No CHE-1152342 and computer resources through the Texas Advanced Computing Center. S.G., H.J., and E.S. would like to acknowledge support from the Icelandic Research Fund and the Eimskip Graduate Fellowship Fund of the University of Iceland.

[1] J. S. Filhol and M. Neurock, Angew. Chem., Int. Ed. **45**, 402 (2006).
[2] M. Otani and O. Sugino, Phys. Rev. B **73**, 115407 (2006).
[3] R. Jinnouchi and A. B. Anderson, J. Phys. Chem. C **112**, 8747 (2008).
[4] E. Skúlason, G. S. Karlberg, J. Rossmeisl, T. Bligaard, J. Greeley, H. Jónsson, and J. K. Nørskov, Phys. Chem. Chem. Phys. **9**, 3241 (2007).
[5] J. Rossmeisl, E. Skúlason, M. E. Björketun, V. Tripkovic, and J. K. Nørskov, Chem. Phys. Lett. **466**, 68 (2008).
[6] V. Tripkovic, E. Skúlason, S. Siahrostami, J. K. Nørskov, and J. Rossmeisl, Electrochim. Acta **55**, 7975 (2010).
[7] E. Skúlason, V. Tripkovic, M. E. Björketun, S. Gudmundsdóttir, G. Karlberg, J. Rossmeisl, T. Bligaard, H. Jónsson, and J. K. Nørskov, J. Phys. Chem. C **114**, 18182 (2010).

[8]V. Tripkovic, M. E. Björketun, E. Skúlason, and J. Rossmeisl, Phys. Rev. B **84**, 115452 (2011).
[9]M. E. Björketun, V. Tripkovic, E. Skúlason, and J. Rossmeisl, "Modeling of the symmetry factor of electrochemical proton discharge via the Volmer reaction," Catal. Today (in press).
[10]J. K. Nørskov, J. Rossmeisl, A. Logadottir, L. Lindqvist, J. R. Kitchin, T. Bligaard, and H. Jónsson, J. Phys. Chem. B **108**, 17886 (2004).
[11]A. Roudgar and A. Gross, Chem. Phys. Lett. **409**, 157 (2005).
[12]J. Rossmeisl, J. K. Nørskov, C. Taylor, M. Janik, and M. Neurock, J. Phys. Chem. B **110**, 21833 (2006).
[13]G. S. Karlberg, J. Rossmeisl, and J. K. Nørskov, Phys. Chem. Chem. Phys. **9**, 5158 (2007).
[14]G. S. Karlberg, T. F. Jaramillo, E. Skúlason, J. Rossmeisl, T. Bligaard, and J. K. Nørskov, Phys. Rev. Lett. **99**, 126101 (2007).
[15]E. Skúlason, T. Bligaard, S. Gudmundsdóttir, F. Studt, J. Rossmeisl, F. Abild-Pedersen, T. Vegge, H. Jónsson, and J. Nørskov, Phys. Chem. Chem. Phys. **14**, 1235 (2012).
[16]A. Hellman *et al.*, J. Phys. Chem. B **110**, 17719 (2006).
[17]W. An and C. H. Turner, Chem. Phys. Lett. **482**, 247 (2009).
[18]C.-C. Wang, S. S. Siao, and J.-C. Jiang, J. Phys. Chem. C **114**, 18588 (2010).
[19]J. Gavnholt, T. Olsen, M. Engelund, and J. Schiøtz, Phys. Rev. B **78**, 075441 (2008).
[20]S.-G. Wang, X.-Y. Liao, D.-B. Cao, C.-F. Huo, Y.-W. Li, J. Wang, and H. Jiao, J. Phys. Chem. C **111**, 16934 (2007).
[21]Y. Liu and J. Wilcox, Environ. Sci. Technol. **45**, 809 (2011).
[22]J. D. Baniecki, M. Ishii, K. Kurihara, K. Yamanaka, T. Yano, K. Shinozaki, T. Imada, K. Nozaki, and N. Kin, Phys. Rev. B **78**, 195415 (2008).
[23]Y. Duan and D. C. Sorescu, Phys. Rev. B **79**, 014301 (2009).
[24]A. A. Peterson, F. Abild-Pedersen, F. Studt, J. Rossmeisl, and J. Nørskov, Energy Environ. Sci. **3**, 1311 (2010).
[25]R. Bader, *Atoms in Molecules: A Quantum Theory* (Oxford University Press, New York, 1990).
[26]P. L. A. Popelier, MORPHY98, a program written by Popelier with a contribution from R. G. A. Bone, UMIST, Manchester, England, 1998.
[27]B. B. Stefanov and J. Cioslowski, J. Comput. Chem. **16**, 1394 (1995).
[28]P. L. A. Popelier, Theor. Chem. Acc. **105**, 393 (2001).
[29]P. L. A. Popelier, Theor. Chim. Acta **87**, 465 (1994).
[30]P. L. A. Popelier, Comput. Phys. Commun. **108**, 180 (1998).
[31]N. O. J. Malcolm and P. L. A. Popelier, J. Comput. Chem. **24**, 437 (2003); **24**, 1276 (2003).
[32]B. P. Uberuaga, E. R. Batista, and H. Jónsson, J. Chem. Phys. **111**, 10664 (1999).
[33]F. W. Biegler-König, J. Schönbohm, and D. Bayles, J. Comput. Chem. **22**, 545–559 (2001).
[34]G. Henkelman, A. Arnaldsson, and H. Jónsson, Comput. Mater. Sci. **36**, 354 (2006).
[35]E. Sanville, S. D. Kenny, R. Smith, and G. Henkelman, J. Comput. Chem. **28**, 899 (2007).
[36]W. Tang, E. Sanville, and G. Henkelman, J. Phys.: Condens. Matter **21**, 084204 (2009).
[37]M. Yu and D. R. Trinkle, J. Chem. Phys. **134**, 064111 (2011).
[38]See http://theory.cm.utexas.edu/bader/ for grid based Bader charge analysis.
[39]S. Gudmundsdóttir, E. Skúlason, and H. Jónsson, Phys. Rev. Lett. **108**, 156101 (2012).
[40]S. Gudmundsdóttir, E. Skúlason, K.-J. Weststrate, L. Juurlink, and H. Jonsson, "Hydrogen adsorption and desorption at the Pt(110)-(1×2) surface: Experimental and theoretical study," Phys. Chem. Chem. Phys. (submitted).
[41]G. Kresse and J. Hafner, Phys. Rev. B **47**, 558 (1993).
[42]G. Kresse and J. Hafner, Phys. Rev. B **49**, 14251 (1994).
[43]G. Kresse and J. Furthmüller, Comput. Mater. Sci. **6**, 16 (1996).
[44]See http://theory.cm.utexas.edu/vtsttools/dos/ for .DOS projection in Bader volumes.
[45]W. Kohn, Rev. Mod. Phys. **71**, 1253 (1999).
[46]See https://wiki.fysik.dtu.dk/dacapo for Dacapo pseudopotential code, Center for Atomic-scale Materials Design (CAMD), Technical University of Denmark, Lyngby.
[47]B. Hammer, L. B. Hansen, and J. K. Nørskov, Phys. Rev. B **46**, 7413 (1999).
[48]P. E. Blöchl, Phys. Rev. B **50**, 17953 (1994).
[49]D. M. Newns, Phys. Rev. **178**, 1123 (1969).
[50]B. Hammer and J. K. Nørskov, Surf. Sci. **343**, 211 (1995).
[51]J. K. Nørskov, private communication (2010–2011).